Hindawi
Advances in Civil Engineering
Volume 2018, Article ID 2948286, 7 pages
https://doi.org/10.1155/2018/2948286

Research Article

Deformation and Stability of Soft Foundation Improved by Prefabricated Vertical Drains Adjacent to River Bank

Changqing Qi, Liuyang Li, and Jiabing Qi

School of Earth Sciences and Engineering, Hohai University, Nanjing 211100, China

Correspondence should be addressed to Changqing Qi; qichangqing79@gmail.com

Received 13 June 2018; Accepted 28 October 2018; Published 14 November 2018

Academic Editor: Damien Rangeard

This paper presents a finite element analysis on a soft embankment foundation improved by prefabricated vertical drains. A plane strain analysis was performed using equivalent permeability. The predictions of settlement, pore water pressure, and lateral displacement were compared with the available field measurement data, and a general fair agreement was observed. Numerical results indicate that the settlement below the left part of the embankment is obviously larger than that of the right part. The maximum settlement occurs below the left shoulder of the embankment and reaches 1.26 m. The entire shallow foundation shows a movement trend to the left toe. The designed left embankment shoulder was suggested to be 0.16 m higher than the right side. Monitoring and simulation results demonstrate that the foundation is stable during the construction. The factor of safety at the end of the final loading stage is about 1.81. The performance of the embankment is consistent with the design prescriptions, confirming the effectiveness of the soil improved technique included in this project.

1. Introduction

The construction of high embankments on soft foundations with a high groundwater level often faces some risks. These risks lie in excessive total and differential settlements, large lateral movement, as well as bearing capacity failure [1]. Thus, the deformation status of soft foundation is one of the main concerns during the construction of infrastructure.

Field measurement traditionally is a practical method to monitor the foundation deformation during construction [2, 3]. But commonly there are only typical sites that are monitored during practical engineering for the lack of funds. The monitored data sometime cannot provide adequate support to the engineering. In order to thoroughly understand the deformation mechanism and predict the stability of the foundation, numerical modeling techniques are useful [4]. Numerical simulation based on laboratory parameters and field measurement results can precisely simulate the deformation behavior of the soft ground. Furthermore, numerical modeling can illustrate the stress-strain status of the soil which is important in bearing capacity failure assessment.

Several numerical approaches have been put into practice for displacement prediction and stress and strain analysis of soft foundation improved with prefabricated vertical drains (PVDs) [5–9]. Most of these models are based on the consolidation theory of Barron [10]. This theory can consider the soil smear effect due to drain installation, drain hydraulic resistance, permeability anisotropy, and so on. The 2D plane strain model developed by Indraratna and Redana [7] was adopted in this paper to perform a full cross-sectional finite element analysis on the stability of the soft foundation underlying a high embankment adjacent to a river bank. The field monitoring data during the construction at a representative cross section were also presented. The monitored data, on one hand, can provide references for the construction. On the other hand, it is the basis for numerical model calibration. On the basis of the calibrated numerical model, the distributions of settlement, lateral displacement, pore water pressure, and the stability status of the foundation were demonstrated.

2. Project Background

The embankment was built along a river bank in Nanjing, China. The existing river bank was designed as a part of the embankment (Figure 1). The embankment is about 8.1 m high with a 42.0 m width top. The slope ratio of the newly built embankment is about 1 : 3.

The foundation soil layers at the monitored site from the original ground surface downward include a 2.0 m thick mucky clay layer, a 17.0 m thick soft silty clay layer, a 9.0 m thick soft to medium clay layer, and an underlying stiff clay layer with unknown thickness. The ordinary groundwater table is about 2 m below the original ground surface.

In order to ensure the stability of the foundation and accelerate the consolidation of the soft soils, the top 2.0 m thick mucky clay layer was first replaced by a fine sand layer. Then PVDs were installed to the bottom of the soft silty clay layer. The drains have a size of 100 mm × 4 mm and were installed in a square pattern with a spacing of 1 m × 1 m. After the installation of PVDs, a coarse sand layer with 1.0 m thick was placed on top of it for the purpose of lateral drainage. The embankment was then constructed layer by layer to the design height, consisting lower fine sand part with a height of 3.8 m and upper clay part of 1.3 m thick.

Numerical predictions and field monitoring were carried out simultaneously during the construction of the embankment. Field measurement results can directly and duly reflect the deformation and safety status of the foundation during embankment construction and also can prove the validity of the calculation procedure. The validated numerical model then can predict the deformation behavior of the embankment foundation and illustrates the distribution characteristics of the deformation. The installation of the measurement instruments is shown in Figure 1. The inclinometer was at the left toe of the embankment, and the settlement plate was on the top of the soft silty clay layer. The piezometers were placed along the centerline of the embankment at depths of 5.0 m below the embankment.

3. Methods and Modeling

3.1. Plain Strain Consolidation Model. The plain strain consolidation model proposed by Indraratna and Redana [7] was used in this paper. This model was verified in many engineering and is easy to be implemented in the finite element approach [7, 11]. In this model, the traditional axisymmetric unit cell (Figure 2(b)) was converted into an equivalent plane strain unit cell (Figure 2(a)) through adjusting the permeability coefficient of the soil between the drain bands. The half width of the plane strain cell was assumed to be the same as the radius of the axisymmetric unit cell:

$$\begin{aligned} D &= R, \\ d_w &= r_w, \\ d_s &= r_s, \end{aligned} \tag{1}$$

where D is the half width of the plane strain unit cell, R is the radius of the axisymmetric unit cell, which equals to the half width of the field spacing of drains; d_w and d_s are, respectively, half width of the drain and smear zone in plane strain unit cell; r_w and r_s are radius of the drain and smear zone in axisymmetric unit cell. According to previous research results, r_s is two to six times of r_w and four to six times is recommended [12]. The radius of drains is given as

$$d_w = r_w = \frac{a+b}{\pi}, \tag{2}$$

where a is the width and b is the thickness of the band drain.

The equivalent plane strain expression of the degree of consolidation at depth z can be expressed as

$$U_{hp} = 1 - \exp\left(\frac{-8T_{hp}}{\mu_p}\right), \tag{3}$$

where T_{hp} is time factor in plane strain model,

$$T_{hp} = \frac{k_{hp}}{m_v r_w}\frac{t}{4D^2}, \tag{4}$$

μ_p can be expressed as follows

$$\mu_p = \left[\alpha + \beta\frac{k_{hp}}{k'_{hp}} + \theta\left(2lz - z^2\right)\right], \tag{5}$$

where k_{hp} is the undisturbed horizontal permeability, k'_{hp} is the smear zone permeability, l is the length of the drain having one-way drainage, and

$$\begin{aligned} \alpha &= \frac{2}{3} - \frac{2d_s}{D}\left(1 - \frac{d_s}{D} + \frac{d_s^2}{3D^2}\right), \\ \beta &= \frac{1}{D^2}(d_s - d_w)^2 + \frac{d_s}{3D^3}\left(3d_w^2 - d_s^2\right), \\ \theta &= \frac{2k_{hp}^2}{k'_{hp}Dq_z}\left(1 - \frac{d_w}{D}\right), \end{aligned} \tag{6}$$

where q_z is the equivalent pane strain discharge capacity of the drain.

For axisymmetric flow in Figure 2(b), the average degree of consolidation at depth z can be represented as

$$\overline{U}_h = 1 - \exp\left(-\frac{8T_h}{\mu}\right), \tag{7}$$

where T_h is the time factor for axisymmetric cell:

$$T_{hp} = \frac{k_h}{m_v r_w}\frac{t}{4R^2}. \tag{8}$$

μ is given by,

$$\mu = \ln\left(\frac{n}{s}\right) + \left(\frac{k_h}{k'_h}\right)\ln(s) - 0.75 + \pi\left(2lz - z^2\right)\frac{k_h}{q_w}, \tag{9}$$

where $n = R/r_w$, $s = r_s/r_w$, k_h and k'_h are the coefficients of horizontal permeability outside and inside the smeared zone, and q_w is the discharge capacity of the drain in axisymmetric cell, $q_w = q_z\pi D/2$.

To maintain the same degree of consolidation at each time step for a given stress level, by equating Equations (3)

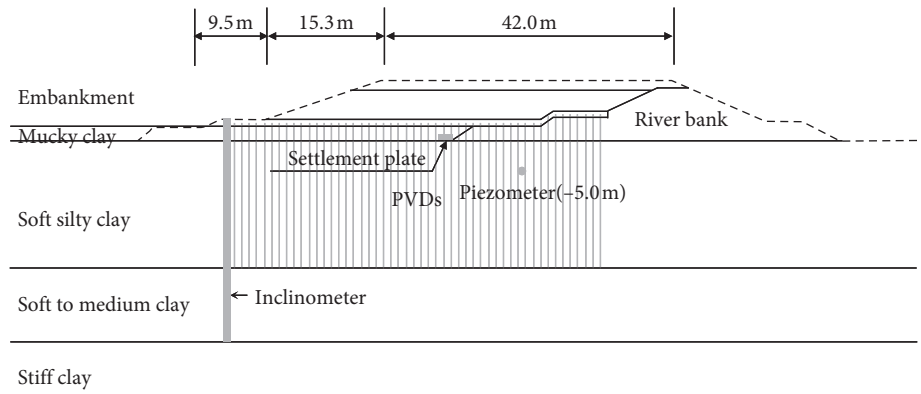

Figure 1: Foundation profile and field instruments arrangement.

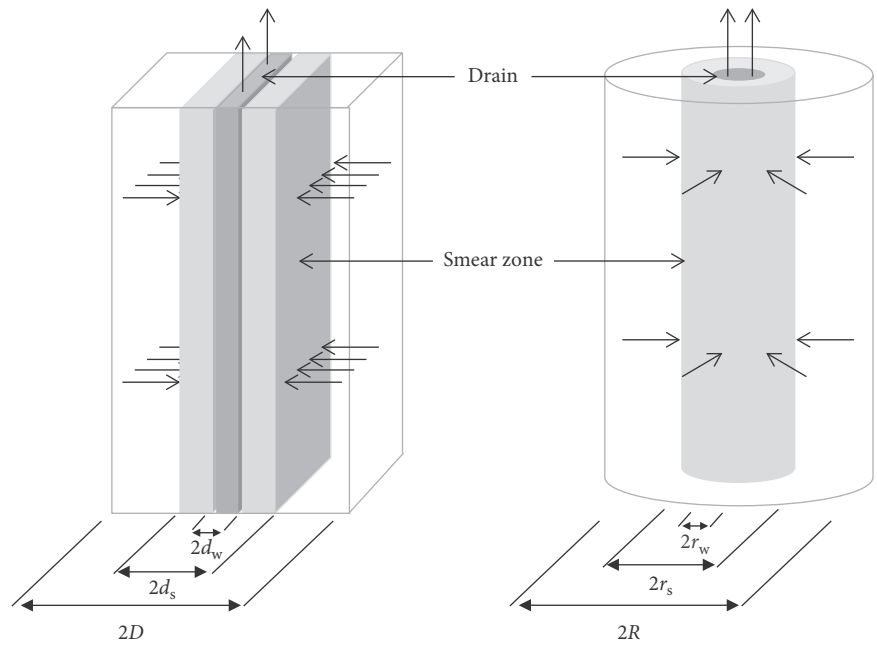

Figure 2: Equivalent plane strain unit cell (a) and axisymmetric unit cell (b) (modified from Reference [7]).

and (7) and combining Equations (4) and (8), the following equation can be obtained:

$$\frac{T_{hp}}{T_h} = \frac{\mu_p}{\mu} = \frac{k_{hp}}{k_h}\frac{R^2}{D^2}. \tag{10}$$

Subsisting Equations (1), (5), and (9) into Equation (10), the following relationship can be obtained:

$$k_{hp} = \frac{k_h\left[\alpha + \beta\left(k_{hp}/k'_{hp}\right) + \theta\left(2lz - z^2\right)\right]}{\ln(n/s) + \left(k_h/k'_h\right)\ln(s) - 0.75 + \pi\left(2lz - z^2\right)\left(k_h/q_w\right)}. \tag{11}$$

If both the smear and well resistance are ignored, Equation (12) can be simplified as

$$k_{hp} = \frac{0.67}{[\ln(n) - 0.75]}k_h. \tag{12}$$

After obtaining k_h and k'_h through experimental test, Equation (12) is accurate enough to determine k_{hp} for plane strain model. Then k'_{hp} can be obtained by Equation (11).

3.2. Finite Element Modeling and Calibration

3.2.1. Finite Element Model and Parameters. The finite element mesh of the simulated embankment is shown in Figure 3. The model includes the existing embankment, the broadened embankment, and foundation. The simulation mainly focused on the deformation characteristics of the region under the embankment, so the horizontal width of the geometry model was chosen as 120 m through trial and comparative method. The bottom of the model is on the top of the stiff clay layer. The lateral boundaries were restrained in horizontal direction, and the bottom boundary was restrained in both horizontal and vertical directions. Drainage boundaries were assumed to be at the level of water table. The lateral and bottom boundaries were kept as undrained. The width of the vertical drains in the equivalent plane strain model is 0.066 m. The width of smear zone is 0.33 m. The width between the drainage bands is 1.0 m. The discharge capability of PVDs was selected as 60 m^3/y in this paper according to the suggestions of the previous literatures

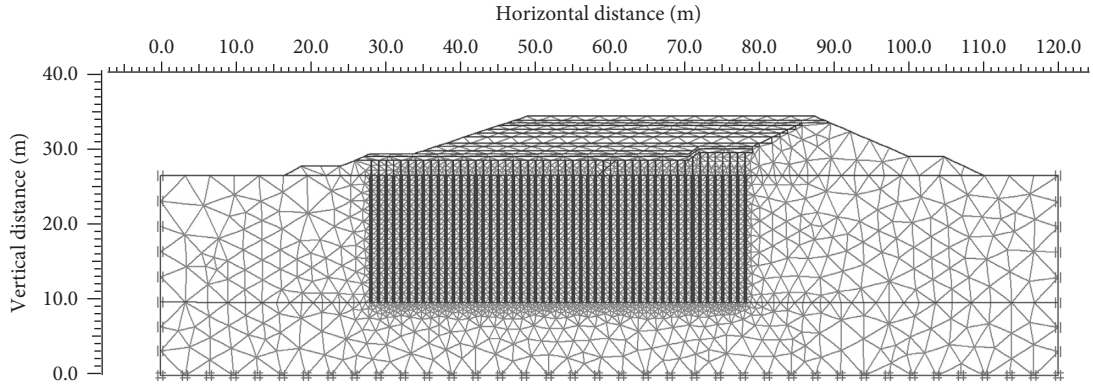

Figure 3: Finite element mesh for plane strain analysis.

[13, 14]. The corresponding permeability for the drain-walls in the full-scale plane strain simulation is 3.05×10^{-5} m/s.

The soft clay creep constitutive model was selected to simulate the behavior of the soft foundation soils. The elastic-perfectly plastic Mohr-Coulomb model was used for embankment fillings. The soil parameters of the subsoil and the embankment fillings are given in Tables 1 and 2, respectively. The plane strain permeability coefficients in the PVDs improved zone are given in Table 3. The permeability coefficients of foundation soils were considered changing with porosity [15]:

$$\log\left(\frac{k}{k_0}\right) = \frac{(e - e_0)}{C_k}, \tag{13}$$

where e_0 is the initial porosity, e is the porosity during consolidation, k_0 and k are the permeability coefficients according to e_0 and e, C_k is the permeability index, and C_k was selected as $0.5e_0$ following the suggestion of Leroueil et al. [16].

3.2.2. Calibration of the Model and Analysis. Figure 4 gives the field measured and simulated time-settlement curves at the monitoring site. The construction process of the embankment is also plotted in Figure 4. It can be observed that the simulated results agree well with the measured data. The model can sufficiently predict the consolidation process of the embankment. It can also be seen that both the simulated and monitored settlement curves follow the loading stages. The settlement curves exhibit two sharp drops during the embankment construction. In the first 36 days, the rapid construction of the sand filling results in a sudden decrease of settlement curves. Then there is a construction break for about 30 days. The second sharp increment of settlement begins from day 70, following a rapid loading rate. After that, the settlement rate reduces smoothly during a slow loading rate. The ground settlement at the monitoring site is about 1.10 m at the end of construction.

The Lateral displacement curves at the end of the construction are shown in Figure 5. It illustrates that the predicted values and the field collected data also fit to each other very well. The lateral displacement increases first with depth and then decreases. The maximum lateral displacement appears at about 5.0 m below embankment toe. The maximum measured lateral displacement is about 196.0 mm at the end of the last loading step.

The measured and the simulated pore water pressures at the measured point are illustrated in Figure 6. The measured and modeled results are closed to each other. The results indicate that PVDs play a noticeable role in controlling the development of excess pore water pressure. The pore water pressure soars sharply during the rapid loading stage and decreases quickly in the loading interval. The pore water pressure in the PVDs improved area reduces smoothly in the latter slow loading stages.

4. Foundation Deformation Profile and Stability

The embankment is composed of newly filled part and the old consolidated river bank. The nonuniform loading leads to asymmetric deformation distribution in the foundation. The modeled settlement profile in the subsoil layers at the end of the construction is illustrated in Figure 7. It indicates that the maximum settlement of the foundation is located below the left shoulder of the embankment, and the settlement develops mainly in the soft silty clay layer. The maximum settlement is about 1.26 m. The different consolidation degree may cause additional differential settlement after construction. In order to ensure the evenness of the embankment, the left embankment shoulder was suggested to be 0.16 m higher than the right side according to our simulation.

The predicted lateral displacement profile at the end of the construction is shown in Figure 8. It can be concluded that the lateral displacement in the subsoil is asymmetry. The new filled embankment gives rise to left ground movement trend during the construction. The maximum lateral displacement is nearly 0.24 m at the end of the construction. The maximum lateral displacement is just below the left toe of the embankment.

The excess pore water pressure distribution at the end of the construction is shown in Figure 9. We can see that PVDs have proper drainage behavior during construction. The excess pore water pressure in the PVDs treatment area is negligible when compared to that of the unimproved area. The maximum value of excess pore water pressure is less than 15.0 kPa in the PVDs area and is still 68.0 kPa in the

Table 1: Summary of the geotechnical properties of subsoil.

Soil	γ (kN/m^3)	e_0	λ^*	κ^*	μ^*	c (kPa)	ϕ (°)	k_h (10^{-9} m/s)	k_v (10^{-9} m/s)
Soft silty clay	17.8	1.61	0.12	0.013	0.002	9.0	15.0	8.62	4.79
Soft to medium clay	18.5	1.2	0.105	0.016	0.001	12.0	18.0	12.0	6.70

γ, unit weight; e_0, initial pore ratio; λ^*, modified compression index; κ^*, modified swell index; μ^*, modified creep index; c, cohesion; ϕ, friction angle; k_h, horizontal permeability; k_v, vertical permeability.

Table 2: Summary of the geotechnical properties of embankment fillings.

Soil	γ (kN/m^3)	E (MPa)	c (kPa)	ϕ (°)	v	k_h (10^{-4} m/s)	k_v (10^{-4} m/s)
Sand filling	16.0	15.6	0	26.0	0.28	1.0	1.0
Clay filling	18.0	3.0	50	18.0	0.30	—	—
River bank clay	18.0	4.3	30	18.0	0.33	—	—
Drainage sand	19.7	14.5	0	32.0	0.25	1.7	1.7

E, Young's modulus; v, Poisson's ratio.

Table 3: Equivalent plane strain permeability of PVD improved soft clay.

Soil	k_{hp} (10^{-9} m/s)	k_{vp} (10^{-9} m/s)	k'_{hp} (10^{-10} m/s)	k'_{vp} (10^{-9} m/s)
Soft silty clay	2.69	1.50	1.4	1.4

k_{hp}, horizontal permeability in undisturbed zone; k_{vp}, vertical permeability in undisturbed zone; k'_{hp}, horizontal permeability in smear zone; k'_{vp}, vertical permeability in smear zone.

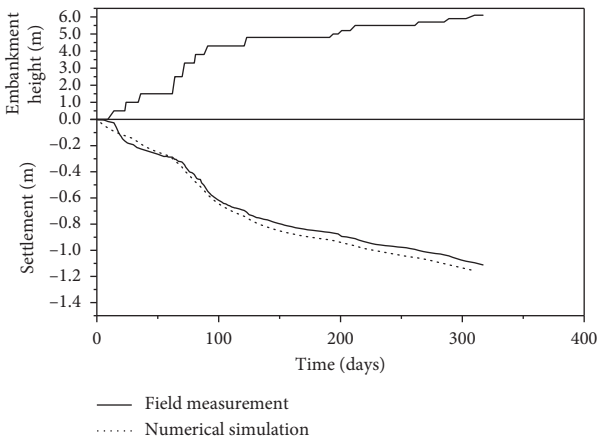

Figure 4: Comparison of measured and simulated settlements at the monitored site.

left unimproved area. This proved that the PVDs have a good effect in accelerating the consolidation and assuring the stability of soft soil. But the large excess pore water pressure below the left toe can cause a long-term post-construction settlement and intensify differential settlement of the foundation. For drainage purpose and enhancing the performance of the embankment, additional PVDs are suggested to be installed in the foundation below the left toe.

The stability of the embankment can be analyzed using the strength reduction method. Figure 10 gives the predicted

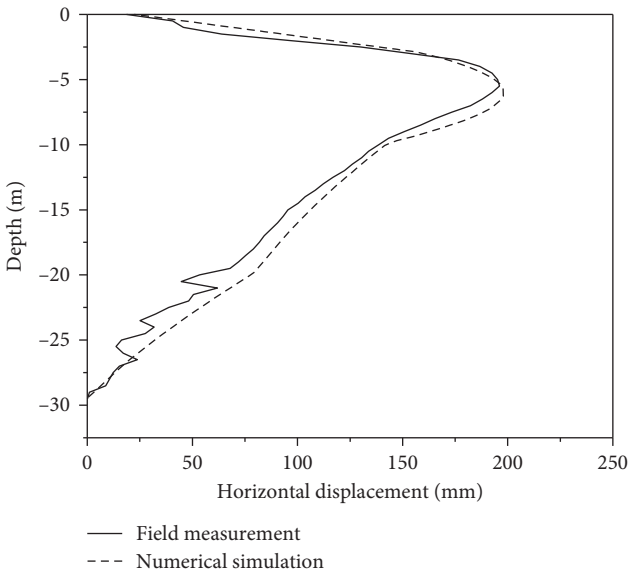

Figure 5: Comparison of measured and predicted lateral displacement.

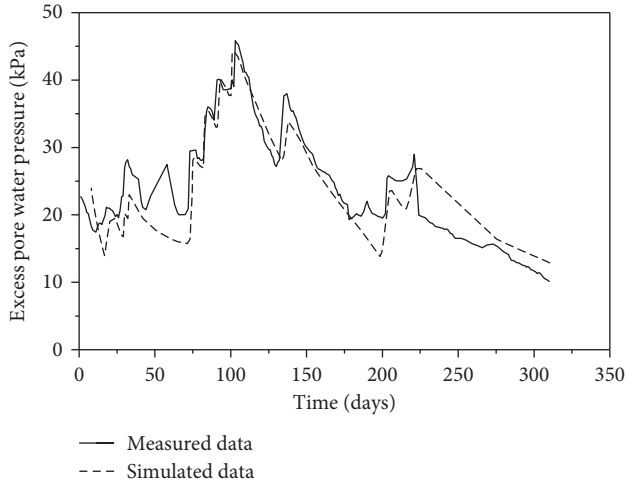

Figure 6: Pore water pressure obtained by field measurement and simulation.

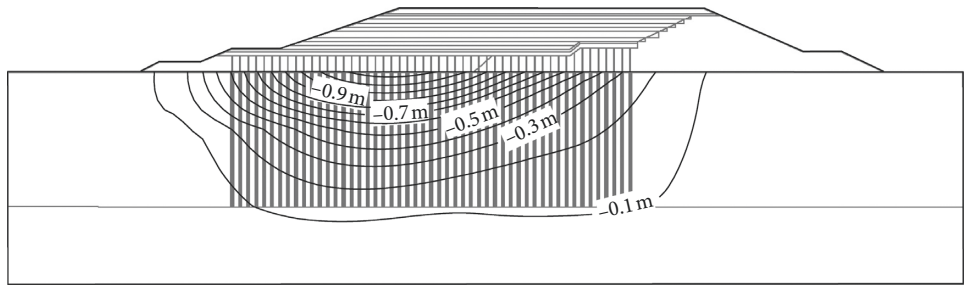

Figure 7: Simulated foundation settlement profile at the end of construction.

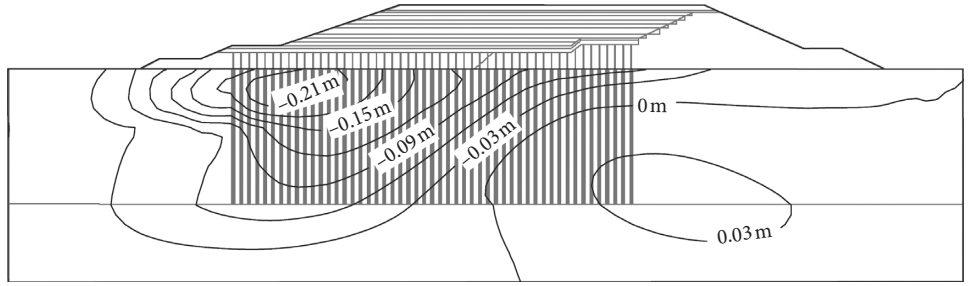

Figure 8: Simulated lateral displacement profile at the end of construction.

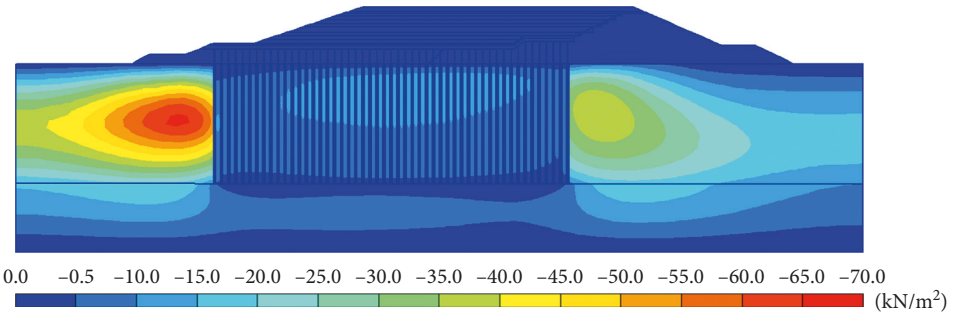

Figure 9: Contour of excess pore water pressure at the end of construction.

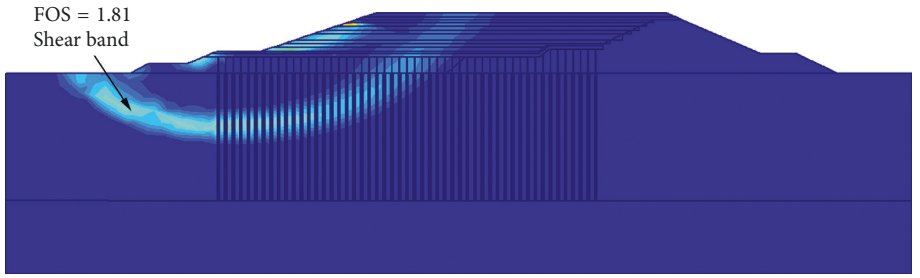

Figure 10: Predicted critical slip surface and factor of safety of the foundation.

shear band based on the maximum incremental shear strain and factor of safety (FOS) at the end of the simulation. The shear band develops from the embankment center to the left toe, and the FOS of the embankment slope is 1.81 at the end of construction. The variation of FOS during construction is given in Figure 11. The FOS decreases sharply during quick loading stages, from 2.05 at the beginning to 1.78 at the end of the quick filling period and then fluctuates during slow loading stages. It indicates the slope is stable enough for the following road crust construction.

5. Conclusions

The deformation behavior of the embankment foundation improved with PVDs was illustrated using the 2D plain strain consolidation model. The numerical simulated results

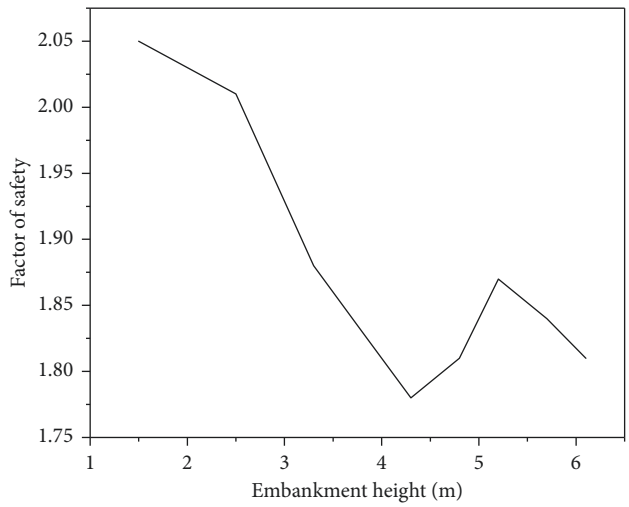

Figure 11: Factor of safety of during the construction.

were compared with the field monitored data. A general fair agreement was observed.

An asymmetric settlement profile was observed in the foundation. The settlement in the left part of the embankment is clearly larger than that of the right part. This behavior was ascribed to the unbalance loading of embankment fillings. The maximum settlement below the left shoulder of the embankment reaches 1.26 m. The left embankment shoulder was suggested to be 0.16 m higher than the right side for the controlling of the differential settlement after construction.

Nearly all the shallow subsoil shows a lateral movement trend to the left toe of the embankment. The maximum lateral deformation measured during the construction is about 0.24 m, occurring below the left toe. The potential shear band obtained by strength reduction method just goes through the bottom of the maximum lateral displacement. The factor of safety decreases during the rapid loading stages and fluctuates during slow loading stages. The factor of safety of the embankment is 1.81 at the end of the last loading stage, thus maintaining a stable status during the construction. The performance of the embankment is consistent with the design prescriptions, which validates the effectiveness of the drainage technique adopted in this project.

Data Availability

The data used to support the findings of this study are included within the article.

Conflicts of Interest

The authors declare that they have no conflicts of interest.

Acknowledgments

The authors greatly appreciate the support provided by the National Natural Science Foundation of China (No. 41877212).

References

[1] P. Wani and V. Sharma, "Improvement of soft soil by using encapsulated and artificially cemented sand column—the review," *International Journal of Computer and Mathematical Sciences*, vol. 7, no. 3, pp. 169–176, 2018.

[2] S. L. Shen, J. C. Chai, Z. S. Hong, and F. Cai, "Analysis of field performance of embankments on soft clay deposit with and without PVD-improvement," *Geotextiles and Geomembranes*, vol. 23, no. 6, pp. 463–485, 2005.

[3] A. Arulrajah, M. W. Bo, M. Leong, and M. M. Disfani, "Piezometer measurements of prefabricated vertical drain improvement of soft soils under land reclamation fill," *Engineering Geology*, vol. 162, pp. 33–42, 2013.

[4] A. Yildiz, "Numerical analyses of embankments on PVD improved soft clays," *Advances in Engineering Software*, vol. 40, no. 10, pp. 1047–1055, 2009.

[5] C. C. Hird, I. C. Pyrah, and D. Russell, "Finite element modelling of vertical drains beneath embankments on soft ground," *Geotechnique*, vol. 42, no. 3, pp. 499–511, 1992.

[6] R. K. Rowe and A. L. Li, "Reinforced embankments over soft foundations under undrained and partially drained conditions," *Geotextiles and Geomembranes*, vol. 17, no. 3, pp. 129–146, 1999.

[7] B. Indraratna and I. W. Redana, "Numerical modeling of vertical drains with smear and well resistance installed in soft clay," *Canadian Geotechnical Journal*, vol. 37, no. 1, pp. 132–145, 2000.

[8] J. C. Chai, S. L. Shen, N. Miura, and D. T. Bergado, "A simple method of modeling PVD improved subsoil," *Journal of Geotechnical and Geoenvironmental Engineering*, vol. 127, no. 11, pp. 965–972, 2001.

[9] C. X. Huang, Y. B. Deng, and F. Chen, "Consolidation theory for prefabricated vertical drains with elliptic cylindrical assumption," *Computers and Geotechnics*, vol. 77, pp. 156–166, 2016.

[10] R. A. Barron, "Consolidation of fine-grained soils by drain wells," *Transactions of American Society of Civil Engineers*, vol. 113, pp. 718–742, 1948.

[11] C. Rujikiatkamjorn, B. Indraratna, and J. Chu, "Numerical modelling of soft soil stabilized by vertical drains, combining surcharge and vacuum preloading for a storage yard," *Canadian Geotechnical Journal*, vol. 44, no. 3, pp. 326–342, 2007.

[12] S. G. Chung and N. K. Lee, "Smear effect and well resistance of PVD-installed ground based on the hyperbolic method," *Journal of Geotechnical and Geoenvironmental Engineering*, vol. 136, no. 4, pp. 640–642, 2010.

[13] R. D. Holtz, M. B. Jamiolkowski, R. Lancellotta et al., *Prefabricated Vertical Drains: Design and Performance*, CIRIA, London, UK, 1991.

[14] B. Indraratna and I. W. Redana, "Plane strain modeling of smear effects associated with vertical drains," *Journal of Geotechnical and Geoenvironmental Engineering*, vol. 123, no. 5, pp. 474–478, 1997.

[15] D. W. Taylor, *Fundamentals of Soil Mechanics*, John Wiley & Sons Inc, Hoboken, NJ, USA, 1948.

[16] S. Leroueil, G. Bouclin, F. Tavenas, L. Bergeron, and P. L. Rochelle, "Permeability anisotropy of natural clays as a function of strain," *Canadian Geotechnical Journal*, vol. 27, no. 5, pp. 568–579, 1990.